ELSEVIER

Atmospheric Research 82 (2006) 173 – 182

ATMOSPHERIC RESEARCH

www.elsevier.com/locate/atmos

Mixing of cloud and clear air in centimeter scales observed in laboratory by means of Particle Image Velocimetry

Piotr Korczyk [a], Szymon P. Malinowski [b,*], Tomasz A. Kowalewski [a]

[a] *Institute of Fundamental Technological Research, Polish Academy of Sciences, Warsaw, Poland*
[b] *Warsaw University, Institute of Geophysics, ul. Pasteura 7, 02-093 Warszawa, Poland*

Accepted 27 September 2005

Abstract

Cloudy air, containing small (∅ 14 μm) water droplets, undergoes mixing with the unsaturated environment inside the cloud chamber in the process resembling smallest scales of entrainment and mixing in real clouds. Particle Image Velocimetry (PIV) applied to images from the chamber interior is used to investigate dynamics of the process in scales from 1.2 mm to few centimeters. A special algorithm, allowing for investigation of droplets motion, is developed, tested and adapted to the experimental data. Two velocity components retrieved in the vertical cross-section through the chamber interior indicate anisotropy of small-scale turbulent motions, with the preferred vertical direction. This result confirms earlier numerical studies, indicating that evaporation of cloud droplets at the cloud–clear air interface may substantially influence the small-scale turbulence in clouds.

Keywords: Atmospheric turbulence; Turbulence in clouds; Small-scale turbulence; Laboratory investigations of atmospheric turbulence; Particle Image Velocimetry

1. Introduction

Interactions between cloud turbulence and microphysics reveal growing attention in recent years. Effect of turbulent velocities and accelerations on the cloud droplet spatial distribution, influence of turbulent mixing of cloud and environment on droplet spectrum evolution are still poorly understood (see e.g. review papers by Pinski and Khain, 1997; Vaillancourt and Yau, 2000; Shaw, 2003). Experimental research in this area is mostly focused on the cloud microphysics only, overlooking adequate information on the small-scale turbulence in clouds. The best available airborne instrumentation for turbulence measurements: aircraft-borne BAT probe (Hacker and Crawford, 1999) or balloon-borne ultrasonic anemometer mounted on ACTOS platform (Siebert et al., 2003) can resolve atmospheric flows down to the scale of order of tens of centimeters. This scale, considered small in typical cloud physics research, is still two orders of magnitude greater than the Kolmogorov microscale or the typical distance between cloud droplets, which both for atmospheric conditions are of order of 1 mm. Thus, atmospheric flow structures in scales crucial for interactions of cloud microphysics and turbulence are not observed in natural conditions.

Consequently, studies of interactions of cloud droplets with turbulence are based on proxy data about in-cloud small-scale turbulence. Such proxy data can be constructed/deduced in few ways: with use of direct numerical simulations (DNS) of turbulent velocity field

* Corresponding author. Tel.: +48 22 55 46 860; fax: +48 22 55 46 882.
E-mail address: malina@fuw.edu.pl (S.P. Malinowski).

0169-8095/$ - see front matter © 2006 Elsevier B.V. All rights reserved.
doi:10.1016/j.atmosres.2005.09.009

in the idealized flow, with use of statistical models of turbulent fluctuations or with adoption of scaling arguments. Koziol and Leighton (1996), Shaw et al. (1998), Vaillancourt et al. (2001, 2002) and Falkovich and Pumir (2004) use DNS results to study various aspects of turbulence/microphysics interactions. Pinsky et al. (2000), Jeffery (2001) and others use statistical models of turbulence to investigate droplet clustering and collision–coalescence processes. Finally, in the paper by Grabowski and Vaillancourt (1999), scaling arguments are used to investigate possible influence of turbulence on microphysics.

In all the above approaches the experimental information about the small scale turbulence comes from the wind tunnel experiments, measurements in the shear-driven turbulence in the atmospheric boundary layer, measurements in clouds in large (of order of meters or more) scales or from heuristic reasoning. Hence, the implicit assumption that in-cloud small-scale turbulence is similar to that in the wind tunnel, or can be deduced from large-scale measurements and simplified phenomenological models of turbulence, affects the results of these works.

In recent years several reports appeared, indicating that in some circumstances a small scale turbulence in clouds may be different than this in the wind tunnel and shear-dominated ABL (atmospheric boundary layer). Grabowski and Clark (1993) show in their numerical experiment that TKE (turbulent kinetic energy) and enstrophy production at the cloud edge are strongly influenced by baroclinic effects at the cloud–clear air interface. Banat and Malinowski (1999) present experimental results that filaments created in the process of turbulent mixing of cloud and clear air are elongated in vertical. They argue that the reason of such behavior is buoyancy force resulting from evaporation of cloud droplets at the border of these filaments. In both above cases the vertical direction is privileged due to the buoyancy forces.

Malinowski and Grabowski (1997) and Malinowski and Jaczewski (1999) present numerical and experimental arguments for importance of relative droplet motion on the process of turbulent mixing of cloud with air. This motion, droplets settling, may form an additional transport mechanism of liquid water from the saturated cloudy filaments to the unsaturated clear air, influencing droplet evaporation. Grabowski and Vaillancourt (1999), on a basis of scaling analysis and Falkovich and Pumir using the numerical modeling, claim that sedimentation is important also for droplet clustering. Note that droplet settling creates preference of the vertical direction yet again.

Verifying above hypotheses Andrejczuk et al. (2004, in press) prove in their high-resolution numerical simulations that in mixing of cloud with clear air turbulent kinetic energy (TKE) is generated in small scales by evaporation of cloud droplets. It leads to anisotropy and confirms that droplet sedimentation is important. An interesting conclusion of this study is that even when production of TKE resulting from evaporative cooling is a small fraction of TKE coming down in the energy cascade from large scales, the resulting small-scale turbulence is anisotropic having a preferred vertical direction. Notice, that so far the small-scale turbulence in clouds was assumed isotropic and it is important to study whether anisotropy may influence droplet collision–coalescence and other microphysical processes in clouds.

In this paper we present the laboratory experiment, which will not answer the above question, but is designed to verify whether this small-scale anisotropy can be observed experimentally. We apply recent advances in full field velocity measurement techniques to the analysis of the laboratory cloud. Our goal is to measure horizontal and vertical motion of cloud droplets at the scale of millimeters and to check, whether small-scale motion of cloud droplets, governed by small-scale turbulence is anisotropic. In the laboratory experiment it is not possible to reproduce all aspects of the in-cloud turbulence, e.g. limited volume of the cloud chamber reduces range of scales present. This means, that results presented below are not fully representative, nevertheless our approach extends the range of the proxy information of the in-cloud turbulence to the area, which was not explored so far.

The adopted laboratory technique is Particle Image Velocimetry (PIV) applied to investigate mixing of droplets with unsaturated air in the cloud chamber. With this technique motion of droplets and consequently properties of the small-scale turbulence can be retrieved. In the following section description of the experiment details on the data processing technique are described. In the fourth section experimental results are presented and discussed. Results are summarized in the last section of the paper.

2. Experiment

In the following experiment we apply improved experimental setup developed by Malinowski et al. (1998) and Jaczewski and Malinowski (2006) to analyze spatial distribution of droplets.

2.1. Experimental system and conditions in the cloud chamber

The experiments are performed in a glass-walled chamber of size $1 \times 1 \times 1.8$ m (Fig. 1). On the top of this chamber a smaller box is located. This box is filled with the artificially generated droplets of the mean diameter of 14.9 ± 5.5 μm (Malinowski et al., 1998). Liquid water load makes the mixture more dense than the environmental air. The cloudy plume of the small negative buoyancy smoothly enters the chamber through the round opening at the upper wall with the velocity of approximately 10 cm s^{-1}. Then turbulence develops and mixing of cloud droplets with air is visualized in the planar cross-section of the chamber using the laser light sheet technique. The plume descends slowly when mixing with the environment, forming turbulent filaments of dry and cloudy air.

Data on the initial velocity of the plume are collected before the imaging, in the additional experimental runs, using a pressure anemometer. In other additional runs cloud droplets in the plume were collected on the oil covered glass and photographed under the microscope in order to estimate the droplet spectrum. Liquid water content of a saturated cloudy plume, estimated on a basis of the droplet spectra and the droplet density calculated from the number of imaged droplets is approximately 4 g kg^{-1}. Temperature of the plume is 22 °C, the same as the initial temperature of the unsaturated (relative humidity $f = 60\%$) in the chamber interior. So far our influence on the initial droplet spectrum and the liquid water content is limited, thus experiments in which sensitivity of the investigated process to the temperature, saturation deficit, liquid water content and droplet spectra cannot be performed in fully controlled manner. In the following we will describe results obtained in the experimental conditions described above.

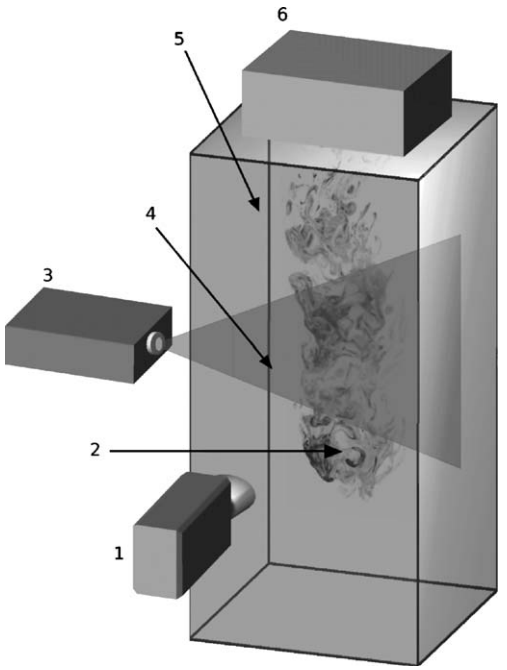

Fig. 1. The experimental setup: 1) CCD camera, 2) cloud during mixing, 3) double-pulse laser, 4) laser sheet, 5) cloud chamber, 6) small chamber with the droplet generator inside.

Tandem of two pulsed lasers (Nd:Yag, wavelength 532 nm) with an energy of 2×36 mJ and repetition rate 12 Hz each is used to illuminate interior of the chamber. An optical system with cylindrical lenses provides 1-mm-thick light sheet of about 15 cm in height. Images of the cloud are observed from the perpendicular direction. For the recording, a high resolution CCD camera (PCO Sensi-Cam) is used in conjunction with a PC Pentium 4/HT computer and a frame grabber. This system provides up to 200 pairs of 1280×1024 pixels 12 bit images, stored in the computer RAM at a rate of 4.5 Hz. The time interval between two laser pulses can be adjusted in order to select the appropriate time delay between the images.

An example of image (negative) from the experiment, covering area of about 7×4.5 cm^2 from the middle part of the chamber is presented in Fig. 2. Inspection of collected images reveals a very fine filamented structure created in the process of turbulent mixing of cloudy plume with unsaturated environment. One pixel in the image corresponds to the volume of about 55×55 μm^2 in the plane of the light sheet and 1 mm deep. Such elementary volumes occupied by droplets are imaged as bright pixels. Due to the properties of Mie scattering, nonuniformity of the light intensity across the light sheet and in the vertical, there is no simple correspondence between the brightness of the pixel and number or size of imaged droplets.

Identification of patterns in the two consecutive images separated by a known time interval allows for determination of two components of motion of the patterns in the plane of the image. This technique, widely adopted in experimental fluid dynamics, is known under name of Particle Image Velocimetry (PIV) (Raffel et al., 1998). To evaluate displacement of traces seeding flow, a pair of images is cross-correlated using small sections of both images, called interrogation windows. The mean displacement is provided for each section by the position of the cross-correlation peak, and velocity in the interrogated region is obtained by dividing the displacement by the time interval. (0.02 s in our case).

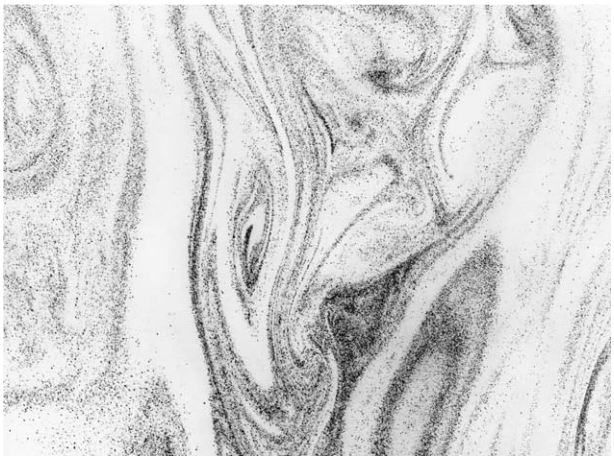

Fig. 2. The negative of the cloud image from the experimental chamber showing small-scale structures created in a process of cloud–clear air mixing. Imaged area corresponds to 7 cm × 4.5 cm in physical space.

Droplets visualized in the chamber differ from typical tracers used for seeding the flow in the standard PIV approach. Cloud droplets are not monodisperse and they are non-uniformly distributed, occupying only part of the PIV image in several distinct filaments. Standard PIV algorithms based on fixed interrogation windows are optimized for the more uniform distribution of markers in the flow and for the less turbulent cases. Such algorithms, initially adopted to retrieve turbulent velocities, produced many artifacts. In order to improve velocity retrieval a special multi-scale algorithm for image processing was developed. This algorithm resembles other multi-scale algorithm described in the literature (Raffel et al., 1998), but is optimized for this particular experimental application. In the chamber condition we evaluate local velocities of cloud droplets with the spatial resolution down to 1.2 mm i.e. close to the Kolmogorov microscale (Fig. 3), in principle better spatial resolution is also possible.

2.2. Details of the data processing

Consider a pair of images collected at a given time interval. Each image is represented by a matrix of the size of 1280 × 1024, equal to the size of the CCD element in the camera. Brightness of each pixel is represented by the 12-bit integer element of the matrix. In order to evaluate displacement of a droplet pattern at position (x,y) a square section of the matrix from the first exposure centered at this position is taken. Then the search of the most similar square sample of the same size in the interrogation area embedded inside the

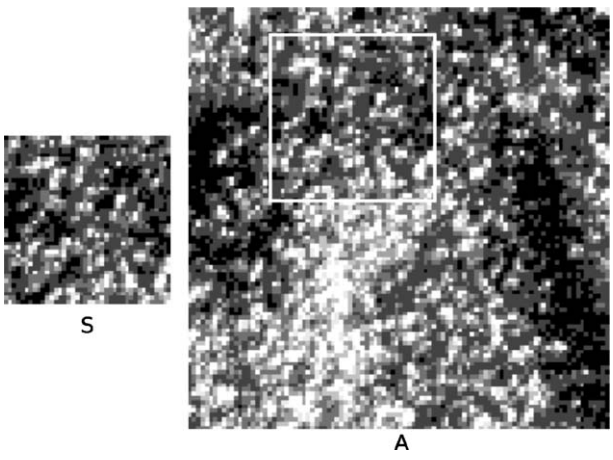

Fig. 3. An example of image section S (40 × 40 pixels) for the first exposure and the corresponding interrogation area A (100 × 100 pixels) for the second exposure extracted from the pair of the images. The most similar part is highlighted.

second exposure is being performed. The size of the interrogation area depends on the expected greatest displacement and on the size of the sample. For a sample S of size $M*M$ and for an interrogation area A of size $L*L$ the evaluation function used to search the most similar sample is defined by the following formula:

$$\phi(m,n) = \sum_{i=1}^{M} \sum_{j=1}^{M} [S(i,j) - \langle S \rangle][A(i+m, j+n) - \langle A \rangle] \tag{2.1}$$

where:

$$\langle S \rangle = \frac{1}{M^2} \sum_{i=1}^{M} \sum_{j=1}^{M} S(i,j) \tag{2.2}$$

$$\langle A \rangle = \frac{1}{M^2} \sum_{i=1}^{M} \sum_{j=1}^{M} A(i+m, j+n) \tag{2.3}$$

For $m \in [0, L-M]$ $n \in [0, L-M]$ the evaluation function can be written as:

$$\phi(m,n) = \sum_{i=1}^{M} \sum_{j=1}^{M} S(i,j) A(i+m, j+n) - M^2 \langle S \rangle \langle A \rangle. \tag{2.4}$$

Maximum of $\Phi(m,n)$ corresponds to best similarity between samples from both exposures, from which displacement of the ensemble of droplets contained in S is evaluated. An example sample, interrogation area and resulting evaluation function is presented in Figs. 3 and 4.

The particular form of $\Phi(m,n)$ was selected from many possible choices (Gui and Merzkirch, 1998) in order to minimize possible errors of the displacement retrievals. The additional advantage of $\Phi(m,n)$ given by (2.4) is that it can be efficiently calculated with the use of the FFT algorithm.

In standard PIV algorithms the choice of the size of a sample is a significant technical problem (Gui and Merzkirch, 1998). In order to overcome this difficulty, the algorithm successively selects smaller and smaller samples. In a first step it looks for the displacement in the whole image in order to remove the bulk motion of the plume. At the next step the size of the sample is reduced and the displacement vector evaluated earlier determines the position of the interrogation area. In this way the displacement is corrected. This algorithm is repeated for a few times with the decreasing size of the sample, giving successive corrections for the velocity in smaller and smaller scales. After such sequence of operations two components of turbulent velocity are evaluated for small patterns. As mentioned, the final spatial resolution corresponds to 1.2 mm.

The obvious limitation of the method is that the retrieved velocity field is limited to the cloudy part of the imaged volume. In the regions with the clear air we do not have information of the turbulent motions. A

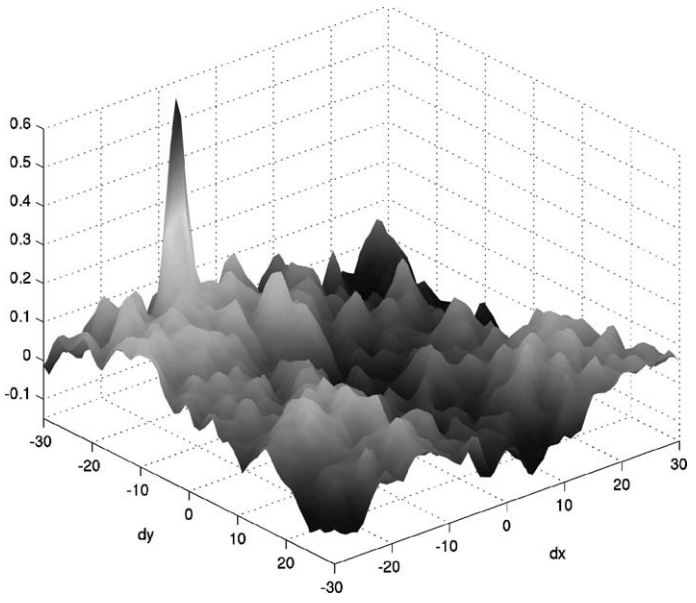

Fig. 4. An example of the evaluation function $\Phi(m,n)$ obtained for the experimental data in Fig. 3.

suitable mask has been created for each scene to depict areas without droplets. This mask has been applied to further statistical analysis of the data. It should be remembered that results given below represent only those parts of the volume where concentration of droplets is sufficient to perform our PIV analysis.

To verify performance and accuracy of the PIV algorithm, it was applied to artificial (benchmark) images with known displacements (Quenot et al., 1998). The accuracy of displacement (velocity) retrieval was estimated from the difference between the known benchmark field of displacements and the evaluated displacements. It was found that the average error of the evaluated displacement is close to 0.5 pixel. For the pixel size of almost 0.06 mm the time interval between exposures of 0.02 s it gives accuracy of the velocity retrieval better than 0.15 mm s^{-1}. The maximum amplitude of turbulent velocities observed during the experiment was around 15 cm s^{-1}, thus the best relative accuracy obtained for measured velocity vector is 0.1%, while the typical relative accuracy (velocities of order of 1.5 cm s^{-1}) is of the order of 1%.

It must be underlined that application of the PIV technique to the cloud droplets, which, due to inertia and gravity, may move with respect to the airflow, causes problem in the interpretation. With the presented approach we do not detect the turbulent velocity of the air, but the velocity of the droplet patterns. Let us briefly discuss possible errors.

Note that the terminal velocity of droplet of 15 μm diameter in air is about 7 mm s^{-1}. If we account for the 50% increase settling velocity due to interaction between droplets in the small-scale turbulence reported by Wang and Maxey (1993), the typical settling velocity of droplets in the chamber is about 1 cm s^{-1}, which is more than the accuracy of the velocity retrieval. Notice, however, that the mean settling velocity of droplets is removed from the data by the substraction of the bulk motion of the plume in the first step of the iterative PIV algorithm. This causes retrieved velocities not being substantially affected by the mean gravitational settling when droplets of various sizes are mixed in space.

Effects of droplet inertia can be well described by the Stokes number, which maximum value should not exceed 0.007 (estimated for 15 μm droplet and for the maximum TKE dissipation rate $\varepsilon = 5 \times 10^{-4}$ m^2 s^{-3} taken from numerical simulations of Andrejczuk et al., submitted for publication). This value suggests that in the experimental conditions motion of droplets does not significantly differ from the motion of surrounding air.

Finally notice that spatial resolution of the retrieved velocity fluctuations is very close to the Kolmogorov microscale, in which we do expect smooth flow of the air. Taking all above into account we conclude that the retrieved velocity field is a reasonable estimate of the turbulent velocity in the cloudy part of the image.

3. Results and discussion

In this section we present statistical properties of horizontal and vertical components of turbulent velocity resulting from analysis of 21 pairs of images (scenes). The imaging area covers about 7 cm × 4.5 cm in the central part of the chamber, about 90 cm below the opening and about 10 cm to the right from the plume

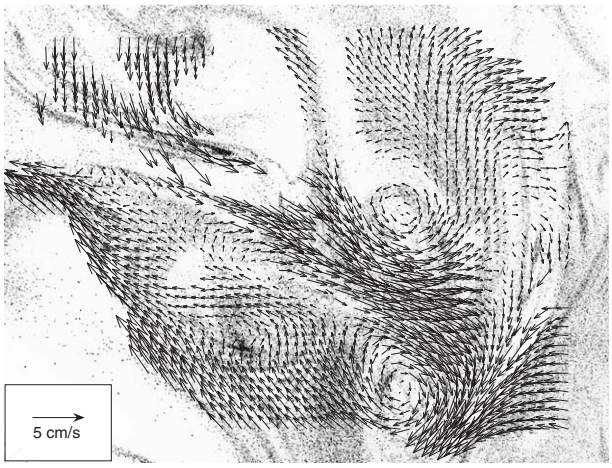

Fig. 5. Velocity field evaluated for the pair of cloud images mapped on one of them; area of about 7 cm × 4 cm is shown.

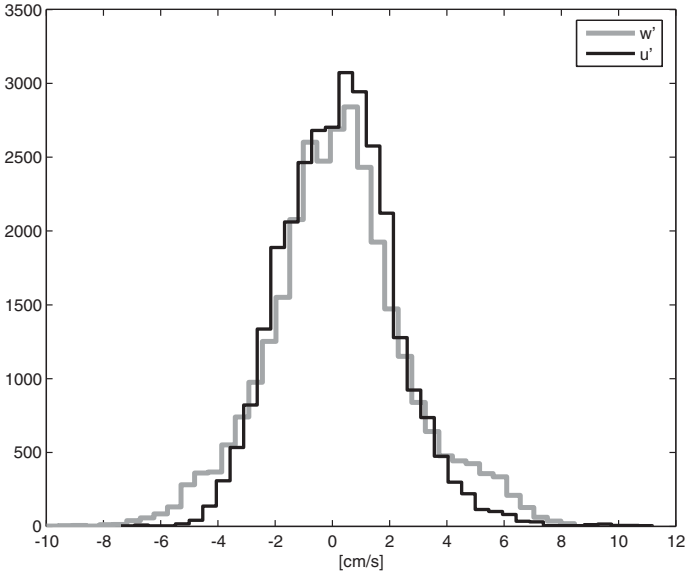

Fig. 6. Histogram of horizontal and vertical turbulent velocities evaluated for all experimental runs.

(chamber) axis. Small imaging area means that in each scene only few (sometimes even one) small-scale turbulent events are captured. Typical interval between the scenes, about 5 s, ensures that each scene is statistically independent from each other. Averaging over all scenes gives the information about the mean properties of the small-scale flow.

Turbulent velocities in each smallest interrogation area of the size of 1.2 mm, which denotes the smallest spatial scale recovered, are calculated according to the equations:

$$u' = u - \overline{u}, w' = w - \overline{w} \tag{3.1}$$

Here u and w are horizontal and vertical velocities estimated in the each smallest interrogation area, dash denotes spatial averaging over the scene, $u'$and w' are corresponding turbulent velocity components. Notice that (3.1) means that statistical properties of turbulence estimated in the experiment are valid for the scale of few (about 4) centimeters and less, down to 1.2 mm. Scales of tens of centimeters, which are present the chamber, are not accounted for.

An example of retrieved turbulent velocities is presented in Fig. 5. Application of Eq. (3.1) ensures that the mean turbulent velocity for each of 21 scenes as well as for the whole ensemble is equal to zero. This is seen in Fig. 6 where histograms of u' and w' from all 21 scenes are plotted. It can be seen that fluctuation velocities greater than 4 cm s^{-1} were observed more often in vertical than in horizontal. This is evident in the analysis of the second, third and fourth statistical moments:

$$\sigma_u = \sqrt{\langle (u')^2 \rangle},\ \sigma_w = \sqrt{\langle (w')^2 \rangle}, \tag{3.2}$$

$$S_u = \frac{\langle (u')^3 \rangle}{\sigma_u^3},\ S_w = \frac{\langle (w')^3 \rangle}{\sigma_w^3}, \tag{3.3}$$

$$K_u = \frac{\langle (u')^4 \rangle}{\sigma_u^4},\ K_w = \frac{\langle (w')^4 \rangle}{\sigma_w^4}, \tag{3.4}$$

of these distributions. In the above <> denotes averaging over all points in which velocity is calculated in all 21 scenes.

Resulting values of statistical moments collected in Table 1 reveal anisotropy of small-scale turbulent motion of cloudy filaments in scale of millimeters: velocity fluctuations in the vertical direction are significantly greater than fluctuations in the horizontal direction. This finding is in agreement with results of Andrejczuk et al. (2004, in press). Small scale mixing

Table 1
Statistics of horizontal and vertical turbulent velocities

	u'	w'
Standard deviation [cm s^{-1}]	1.9	2.4
Skewness	0.39	0.17
Kurtosis	3.9	3.5

patterns created by such anisotropic velocity distribution can be elongated in vertical, as was shown by Banat and Malinowski (1999). This vertical elongation can be observed in Fig. 2 and in many other images from the experiment.

An additional comment is required in order to understand the positive skewness of both distributions of u' and w'. The imaged volume of the cloud chamber is shifted right from the axis of the chamber. This means that the field of view of the camera is closer to the right edge of the negatively buoyant cloudy plume. Such plumes are characterized by the entraining, rotating eddies and the certain profile of vertical velocity (maximum negative value on the axis) and transport of the material from the plume interior outwards. Notice that turbulent velocities are calculated for the cloudy filaments only, clear ones do not count. Additionally the mean vertical velocity is substracted. Thus, positive skewness of u' and w' in the data does not mean that the whole velocity field has this property.

Kurtosis of u' and w' indicate longer tails and narrower centers of the distributions than for the Gaussian one. It is possible that this property of the distribution is related to the TKE production by the evaporative cooling at the edges of the cloudy filaments, which was reported by Andrejczuk et al. (2004). Again, this corresponds to the motion of cloudy filaments only.

In order to compare anisotropy of the observed flow to this reported by Andrejczuk et al. (2004), Taylor micro-scales (horizontal and vertical) are calculated according to the following definitions:

$$\lambda_u = \frac{\langle (u')^2 \rangle^{1/2}}{\left\langle \left(\frac{\partial u'}{\partial x}\right)^2 \right\rangle^{1/2}}, \quad \lambda_w = \frac{\langle (w')^2 \rangle^{1/2}}{\left\langle \left(\frac{\partial w'}{\partial z}\right)^2 \right\rangle^{1/2}}. \tag{3.5}$$

Velocity derivatives are calculated from the experimental flow field using the simplest two-point algorithm. The resulting values of Taylor microscales are: $\lambda_u = 5.83 \pm 0.23$ mm and $\lambda_w = 6.92 \pm 0.36$ mm. Similarly to Andrejczuk et al. (2004, submitted for publication), the vertical Taylor microscale is larger than the horizontal one, however these experimental values are few times smaller than reported in their studies. The possible explanation is that velocity derivatives are estimated here on 0.12 cm grid, while they used computational grid of 1 cm size (2004 report) and 0.25 cm (2006 report).

Statistical information of the flow observed in the chamber is collected in Table 2. In the second and third columns the mean squared horizontal and vertical turbulent velocity components in cloudy filaments are presented for all the scenes. It can be seen that in 16 of 21 scenes and for the all scenes $\overline{(w')^2} > \overline{(u')^2}$, which confirms anisotropy with the preferred direction in vertical.

Table 2
Properties of turbulent flow observed in the chamber

Scene no.	$\overline{(u')^2}$ [10^{-4} m^2 s^{-2}]	$\overline{(w')^2}$ [10^{-4} m^2 s^{-2}]	E [10^{-4} m^2 s^{-2}]	Ω [s^{-2}]	Re_λ
1	2.3	6.4	5.5	29.3	12.4
2	3.4	1.1	3.9	17.2	11.5
3	2.4	2.9	3.8	27.7	8.9
4	5	6.7	8.3	71.3	12
5	7.1	15.3	14.7	64.6	22.3
6	4	11.7	9.9	80.8	13.4
7	4.7	3.8	6.6	55.3	10.9
8	8.1	6.7	11.5	88.6	14.8
9	2.6	5.6	5.4	27.2	12.5
10	1.5	2.8	2.9	17.5	8.5
11	3.7	2.8	5.1	41.7	9.5
12	2.6	5.1	5.1	50.6	8.8
13	4.3	14.5	11.5	70.4	16.7
14	4	8.1	8.1	32.3	17.3
15	2.3	4.3	4.5	26.5	10.5
16	2.6	5.1	5.2	32.9	11
17	2.1	4.8	4.6	41.1	8.7
18	3.5	5.6	6.3	66.4	9.4
19	3	1.6	3.8	18.2	10.8
20	7.1	2.2	8.2	45.8	14.7
21	5.7	7.4	9.4	80.5	12.8
Average	3.9	5.9	6.9	46.9	12.3

In the fourth column the turbulent kinetic energy in the scales of few centimeters and less is estimated, assuming horizontal isotropy of the motion in each scene:

$$E = \frac{1}{2}\left[2\overline{(u')^2} + \overline{(w')^2}\right] \tag{3.6}$$

Enstrophy, shown in the following column, is estimated from:

$$\Omega = \frac{3}{2}\overline{\omega^2}, \tag{3.7}$$

in which isotropy of the vorticity vector has been assumed. This assumption is probably not very good, but allows for the qualitative estimate of the Taylor microscale Reynolds number from the relation:

$$Re_\lambda = \frac{E}{\nu}\left(\frac{10}{3\Omega}\right)^{\frac{1}{2}}, \tag{3.8}$$

where ν is the kinematic viscosity of the air. Notice, that small values of Re_λ in Table 2, suggesting very weak turbulence can be misleading, due to accounting only

TKE energy of the smallest scales of motion, which usually contain only a small fraction of the whole TKE.

4. Summary and conclusions

Our study demonstrates the possibility of using Particle Image Velocimetry for quantitative analysis of cloud droplets motion inside the cloud chamber. In the absence of large droplets and high accelerations the retrieved velocity field exhibit characteristics of the small-scale velocity field inside the cloudy filaments. Statistical analysis of the retrieved velocity field confirms suggestion of earlier numerical simulations, that small scales anisotropy of the turbulence takes place in regions of entrainment and mixing of cloud filaments with clean air. This finding can potentially be important for understanding the collision–coalescence of droplets as well as details of the mixing process in clouds. Whether and how accounting anisotropy would help in understanding the warm rain initiation is a matter of future studies. We should be aware, however, that the experimental information we gather in horizontal, when flying through clouds, may not be enough to properly describe complicated processes which govern cloud turbulence/microphysics/thermodynamics interactions.

The analysis presented here is valid for the smallest scales of turbulent motions only. It should also be underlined that by the principle of the measurements results are valid for the cloud filaments, velocities inside the clear air filaments are not measured. Thus, direct comparison of our results to other experimental and numerical data, covering larger scales of motion and both cloudy and clear air regions, is not simple. On the other hand, the presented study is unique in a sense that it gives an experimental information on the smallest scales of turbulence, in which interaction with cloud microphysics takes place.

The present setup of the experiment has its limitations. In the future authors plan to improve the measurement technique in order to:

- investigate the anisotropy in a function of the distance from the inlet to the main chamber in order to understand possible effect of initial anisotropy, droplet settling and the temporal evolution of the cloud–clear air mixing;
- investigate the influence of liquid water content in the plume and saturation deficit in the clear air on anisotropy;
- perform the additional series of experiments with dry particles in place of water droplets in order to quantify effects of evaporation and effects of particle–flow dynamical interactions.

Acknowledgments

This research was supported by a research grant no. 5 T07A 052 24 from the Polish Committee for Scientific Research. Authors thank the anonymous reviewers for their comments and suggestions.

References

Andrejczuk, M., Grabowski, W.W., Malinowski, S.P., Smolarkiewicz, P.K., 2004. Numerical simulation of cloud–clear air interfacial mixing. J. Atmos. Sci. 61, 1726–1739.

Andrejczuk, M., Grabowski, W.W., Malinowski, S.P., Smolarkiewicz, P.K., in press. Numerical simulation of cloud–clear air interfacial mixing: Convergence study and turbulence impact on cloud microphysics. J. Atmos. Sci.

Banat, P., Malinowski, S.P., 1999. Properties of the turbulent cloud–clear air interface observed in the laboratory experiment. Phys. Chem. Earth: Part B. Hydrol. Oceans Atmos 24, 741–745.

Falkovich, G., Pumir, A., 2004. Intermittent distribution of heavy particles in a turbulent flow. Phys. Fluids 16, L47–L50.

Gui, L., Merzkirch, W., 1998. Generating arbitrarily sized interrogation windows for correlation-based analysis of Particle Image Velocimetry recordings. Exp. Fluids 24, 66–69.

Grabowski, W.W., Clark, T.L., 1993. Cloud–environment interface instability: Part II. Extension to three spatial dimensions. J. Atmos. Sci. 50, 555–573.

Grabowski, W.W., Vaillancourt, P.A., 1999. Comments on "preferential concentration of cloud droplets by turbulence: effects on the early evolution of cumulus cloud droplet spectra". J. Atmos. Sci. 56, 1433–1436.

Hacker, J.M., Crawford, T.L., 1999. The BAT-probe: the ultimate tool to measure turbulence from any kind of aircraft (or sailplane). J. Tech. Soar. XXIII (2), 43–46.

Jaczewski, A., Malinowski, S.P., 2006. Spatial distribution of cloud droplets in a turbulent cloud chamber flow. Q. J. Roy. Meteorol. Soc. 131, 2047–2062.

Jeffery, C.A., 2001. Investigating the small-scale structure of clouds using the δ-correlated closure: effect of particle inertia, condensation/evaporation and intermittency. Atmos. Res. 59–60, 199–215.

Koziol, A.S., Leighton, H.G., 1996. The effect of turbulence on the collision rates of small cloud drops. J. Atmos. Sci. 53, 1910–1920.

Malinowski, S.P., Grabowski, W.W., 1997. Local increase in concentration of cloud droplets and water content resulting from turbulent mixing. J. Tech. Phys. 38, 397–406.

Malinowski, S.P., Jaczewski, A., 1999. Laboratory investigation of the droplet concentration at the cloud–clear air interface. Phys. Chem. Earth: Part B. Hydrol. Oceans Atmos 24, 477–480.

Malinowski, S.P., Zawadzki, I., Banat, P., 1998. Laboratory observations of cloud–clear air mixing in small scales. J. Atmos. Ocean. Technol. 15, 1060–1065.

Pinsky, M.B., Khain, A.P., 1997. Turbulence effects on droplet growth and size distribution in clouds—a review. J. Aerosol Sci. 28, 1177–1214.

Pinsky, M.A., Khain, A.P., Shapiro, M., 2000. Stochastic effects of cloud droplet hydrodynamic interaction in a turbulent flow. Atmos. Res. 53, 131–169.

Quenot, G.M., Pakleza, J., Kowalewski, T.A., 1998. Particle Image Velocimetry with optical flow. Exp. Fluids 25, 177–189.

Raffel, M., Willert, Ch.E., Kompenhans, J., 1998. Particle Image Velocimetry: A Practical Guide. Springer, ISBN 3540636838. 253 pp.

Shaw, R.A., 2003. Particle–turbulence interactions in atmospheric clouds. Annu. Rev. Fluid Mech. 35, 183–227.

Shaw, R.A., Reade, W.C., Collins, L.R., Verlinde, J., 1998. Preferential concentration of cloud droplets by turbulence: Effects on the early evolution of cumulus cloud droplet spectra. J. Atmos. Sci. 55, 1965–1976.

Siebert, H., Wendisch, M., Conrath, T., Teichmann, U., Heintzenberg, J., 2003. A new tethered balloon-borne payload for fine-scale observations in the cloudy boundary layer. Boundary - Layer Meteorol. 106, 461–482.

Vaillancourt, P.A., Yau, M.K., 2000. Review of particle–turbulence interactions and consequences for cloud physics. Bull. Am. Meteorol. Soc. 81, 285–298.

Vaillancourt, P.A., Yau, M.K., Grabowski, W.W., 2001. Microscopic approach to cloud droplet growth by condensation. Part I: model description and results without turbulence. J. Atmos. Sci. 58, 1945–1964.

Vaillancourt, P.A., Yau, M.K., Bartello, P., Grabowski, W.W., 2002. Microscopic approach to cloud droplet growth by condensation: Part II. Turbulence, clustering, and condensational growth. J. Atmos. Sci. 59, 3421–3435.

Wang, Lian-Ping, Maxey, M.R., 1993. Settling velocity and concentration distribution of heavy particles in homogeneous isotropic turbulence. J. Fluid Mech. 256, 27–68.